SUPPLEMENTARY MATERIALS AND METHODS

Mice. TAL-deficient mice were developed by inactivation of the TALDO1 genomic locus (1). TAL-/- male mice are infertile due to sperm dysmotility associated with loss of the mitochondrial transmembrane potential ($\Delta\psi_m$)(1). Therefore, TAL-deficient mice have been generated through breeding heterozygotes and tail tissue typing by PCR and Western blot analysis of TAL expression (1). Between 2001-2004, TAL+/- mice have been back-crossed onto the C57BL/6 background for >11 generations. Congenic C57BL/6 heterozygotes (TAL+/-) have been bred for comparative analysis of mice with complete (TAL-/-) and partial TAL deficiency (TAL+/-) relative to wild-type littermates (TAL+/+). Among 692 pups born to heterozygote parents, the proportion of wild-type (168/692, 24.4%), heterozygote (355/692, 51.3%) and homozygote knockout genotypes (169/692, 24.4%) did not significantly differ from the expected Mendelian inheritance.

In vivo treatments. Fas-induced apoptosis was induced by intraperitoneal injection of 10 µg of Fas-specific Jo2 hamster monoclonal antibody (BD Pharmingen Cat. No. 554254, San Diego, CA) in 100 µl of phosphate-buffered saline (PBS) per 30 g of body weight. Acetaminophen APAP (acetyl-p-aminophenol or APAP) was injected ip at doses ranging between 100-800 mg/kg. Fas or APAP-treated mice were continuously monitored and euthanized at predetermined time points or the earliest sign of distress. N-acetylcysteine (NAC, Sigma Ultragrade, 10 mg/ml pH 6.7) was administered in the drinking water. To test glucose tolerance, after fasting overnight (~14h), mice were injected ip with sterile-filtered 10% glucose in 0.9% NaCl at a dose of 2 g/kg.

Tail vein blood drops were obtained with needle pricking, before and 15, 30, 60, and 120 min after glucose injection. A single drop of blood was used to assess glucose level with a OneTouch Ultra electronic blood glucose monitor (LifeScan), as earlier described (2).

Liver pathology. Paraffin-embedded sections were stained with hematoxylin-eosin (H&E) and evaluated blindly to the genotype by Dr. Steven Landas for dysplasia, cirrhosis, and HCC on the basis of established criteria (3-5). Clearly circumscribed nodular lesions with dysplastic cells, small cell change, or large cell change were regarded as dysplastic nodules. Only lesions with definitive invasion, manifested by irregular and infiltrative interface into the adjacent liver were regarded as carcinoma. No adenomas were observed. Fat-storing hepatic stellate or Ito cells were identified by staining with antibody to glial fibrillary acidic protein (GFAP) (6). Fat deposition and fibrosis were detected by Oil-Red-O (ORO) and Klatskin's trichrome staining, respectively.

Apoptosis of liver cells of Fas antibody-injected animals was assessed by TUNEL staining using the In Situ Cell Death Detection kit from Roche (Indianapolis, IN). Paraffin-embedded liver sections were de-paraffinized, rehydrated, and labeled with fluorescein-dUTP using terminal deoxynucleotidyl transferase (TdT). During this incubation period, TdT catalyzes the addition of fluorescein-dUTP at free 3'-OH groups in single- and double-stranded DNA breaks. After washing, the label incorporated at the damaged sites of the DNA is marked by an anti-fluorescein antibody conjugated with the reporter enzyme alkaline phosphatase (AP). After washing to remove unbound enzyme conjugate, the AP retained in the immune complex at the site of the damaged DNA was visualized by addition Vector Black AP Substrate (Vector Labs). Expression of proliferating cell nuclear antigen (PCNA) was detected with mouse monoclonal antibody from

BDBiosciences (Cat no: 610664).

Electron microscopy. Freshly excised tissues were fixed overnight in phosphate-buffered saline with 2.5% glutaraldehyde, postfixed in 1% OsO_4, dehydrated in graded ethanol series, infiltrated with propylene oxide and embedded in Araldite 502 epoxy resin. Ultrathin sections were stained with uranyl acetate and Reynold's lead citrate prior to examination using a Tecnai BioTWIN 12 transmission electron microscope (FEI).

Isolation and in vitro culture of mouse hepatocytes. Livers of 8- to 10-week-old TAL+/+, TAL+/-, and TAL-/- female littermates were canulated through the portal vein, and after nicking the inferior vena cava, perfused by a two-step procedure using Ca^{2+}-free pre-perfusion buffer and perfusion medium with 0.02 % type IV collagenase and 0.4U/ml elastase (both from Sigma), as previously described (7). Isolated hepatocytes with viability exceeding 90% were resuspended in DMEM containing 100 IU/ml penicillin G, 100 µg/ml streptomycin, 0.2 mg/ml serum bovine albumin, 1 mM sodium pyruvate and 10% fetal calf serum and kept on ice until staining for flow cytometry. For in vitro culture, 2.4 x 10^6 hepatocytes were plated in 60 mm Petri-dishes pre-coated with type I collagen (Sigma, Cat No. C9791). After 3 h incubation, plates were washed and incubated for 6 h with fresh DMEM medium and used for in vitro nitrite assays using the Griess kit (Eugene, OR). For Fas-induced apoptosis, 2.4 x 10^6 hepatocytes were plated in collagen-coated 24-well plates. After 3 h incubation, plates were washed and incubated for 8 h with anti-Fas antibody (Jo2, 0.5 µg/ml) and 50 µg/ml cycloheximide (Cyc) or 50 ng/ml actinomycin D (AcD) (8). Control cultures were incubated with DMEM medium, Cyc, or AcD

only. Caspase 3 activity of cell supernatants was measured by the DEVD-AFC cleavage assay (9).

Flow cytometric analysis of $\Delta\psi_m$, mitochondrial mass, NO and ROI production, GSH, cytoplasmic and mitochondrial Ca^{2+} levels. Hepatocytes were analyzed on a Becton Dickinson LSRII flow cytometer equipped with 20 mW solid-state Nd-YAG (emission at 355 nm), 20 mW argon (emission at 488 nm) and 16 mW helium-neon lasers (emission at 634 nm). Dead cells and debris were excluded from the analysis by electronic gating of forward (FSC) and side scatter (SSC) measurements. Each measurement was carried out on 10,000 cells. Mitochondrial transmembrane potential ($\Delta\psi_m$) was estimated by staining for 15 min at 37°C with cationic lipophilic dye 20 nm 3,3'-dihexyloxacarbocyanine iodide ($DiOC_6$, Molecular Probes, Eugene, OR; excitation: 488 nm, emission: 525 nm recorded in FL-1). Fluorescence of $DiOC_6$ is oxidation-independent and correlates with $\Delta\psi_m$ (10). $\Delta\psi_m$ was also quantitated using a potential-dependent J-aggregate-forming lipophilic cation, 5,5',6,6'-tetrachloro-1,1',3,3'-tetraethylbenzimidazolocarbocyanine iodide (JC-1) (11). JC-1 selectively incorporates into mitochondria, where it forms monomers (fluorescence in green, 527 nm) or aggregates, at high transmembrane potentials (fluorescence in red, 590 nm) (11) (12) (13). $\Delta\psi_m$ relative to mitochondrial mass was assessed by JC-1 FL-2/FL1 fluorescence(13). Cells were incubated with 0.5 μM JC-1 for 15 min at 37°C before flow cytometry. $\Delta\psi_m$ changes were also confirmed by staining with 1 μM CMXRos (excitation: 579 nm, emission: 599 nm recorded in FL-2) and 1 μM TMRM (excitation: 543 nm, emission: 567 nm recorded in FL-2; all from Molecular Probes). Co-treatment with a protonophore, 5 μM carbonyl cyanide m-chlorophenylhydrazone (mClCCP, Sigma) for 15 min at 37°C resulted in decreased $DiOC_6$, CMXRos, TMRM, and JC-1

fluorescence and served as a positive control for disruption of $\Delta\psi_m$ (9). Mitochondrial mass was monitored by staining with potential-insensitive mitochondrial dyes 50 nM nonyl acridine orange (NAO, excitation: 490 nm, emission: 540 nm recorded in FL-1) or 100 nM MitoTracker Green-FM (excitation: 490 nm, emission: 516 nm recorded in FL-1; Molecular Probes).

NO production was assessed by DAF-FM fluorescence in annexin V-Alexa-647-negative cells, as earlier described (14). NO levels were also assessed in the supernatant of hepatocytes cultured on collagen-coated plate by the Griess reaction using the nitrite detection kit from Molecular probes.

Production of ROI was assessed fluorometrically using oxidation-sensitive fluorescent probes 5,6-carboxy-2',7'-dichlorofluorescein-diacetate (DCFH-DA), dihydrorhodamine 123 (DHR) and dihydroethidium (hydroethidine, DHE; Molecular Probes) as earlier described (9;15). Fluorescence emission from 5,6-carboxy-2',7'-dichlorofluorescein (DCF; green) or DHR (green) was detected at a wavelength of 530 ± 30 nm. Fluorescence emission from oxidized HE, ethidium (red), was detected at a wavelength of 605 nm. While R123, the fluorescent product of DHR oxidation, binds selectively to the inner mitochondrial membrane, the oxidized products of DCFH-DA and DHE, ethidium and dichlorofluorescein (DCF), respectively, remain in the cytosol of living cells. DCF and DHE preferentially detect H_2O_2 and superoxide (O_2-), respectively (16-18). Intracellular GSH levels were assessed with 100 μM monochlorobimane (MCB, excitation: 380 nm/emission: 461 nm; FL-UV) (1).

Cytoplasmic calcium concentration was assessed by loading the cells with 1 μM Fluoro-3/AM (excitation: 506 nm, emission: 526 nm recorded in FL-1; Molecular Probes). After entering the cell, AM hydrolysis occurs and, thereafter, the dye is caged in the cell. Fluo-3 exhibits large

fluorescence intensity increase on binding calcium. Mitochondrial calcium level was estimated by loading the cells with 4 μM rhod2/AM which is compartmentalized into the mitochondria (19).

Lipid hydroperoxide (LPO) assay. LPO levels were measured with a kit from Calbiochem/EMD Biosciences (Cat. No. 437639). Triplicates of liver tissues (~200 mg) were homogenized in 500 μl of HPLC-grade autoclaved water and, after addition of 500 μl of extract-R-saturated methanol, extracted with 1 ml of deoxygenated chloroform. 700 μl of interface-free chloroform extract was assayed for LPO content relative to a standard calibration curve following the manufacturer's instructions. LPO levels were expressed in pmol/mg protein.

Western blot analyses. Protein lysates of freshly excised tissue were prepared by sonication using a Fisher Model 100 Sonic Dismembrator (Fisher Scientific, Pittsburgh, PA) in 300 μl of buffer containing 20 mM Tris-HCl (pH 7.5), 150 mM NaCl,1 mM Na_2EDTA,1 mM EGTA, 1% Triton, 2.5 mM sodium pyrophosphate, 1 mM beta-glycerophosphate,1 mM Na_3VO_4, 1 μg/ml leupeptin. Protein concentrations were determined by the Bradford method using the Bio-Rad Protein Assay (Bio-Rad Laboratories, Hercules, CA). 40 μg of protein lysates, unless otherwise indicated, were separated on a 12% SDS-polyacrylamide gel and electroblotted to nitrocellulose. TAL was detected antibody 170 (20). β-actin was assessed with mouse Ab 1501R (Chemicon, Temecula, CA), as previously described (20). Western blot detection of c-jun, was performed using c-jun rabbit antibody from Upstate Biotechnology (Cat. No 06-225). Alpha-fetoprotein (AFP) was detected with a mouse monoclonal antibody (R&D Systems; Cat No. MAB 1368). Aldose reductase (AR) was detected with a rabbit antibody kindly provided by Kenneth H.

Gabbay (21). Phosphorylated c-jun levels were assessed using Ser63-phospho-c-jun antibody (Cell Signaling Cat.No. 9261). Antibodies to the 46 kD and 54 kD isoforms of c-jun N-terminal kinase (JNK) were obtained from Santa Cruz (Cat.No. sc-571). Antibodies to the phosphorylated forms of JNK were obtained from Cell Signaling (Cat.No.4668). β-catenin-specific monoclonal antibody was obtained from BDBiosciences (Cat. No. 610154). Phospho-β-catenin (Thr41/Ser45) specific rabbit antibody was obtained from Cell Signaling (Cat.No.9565S). Malondialdehyde (MDA) adducted proteins were detected with a rabbit antibody from Calbiochem/EMD Biosciences (Cat. No. 442730) or goat antibody from Santa Cruz (Cat. No. sc-130087). 4-hydroxynonenal (4-HNE) adducted proteins were detected with a rabbit antibody from Alexis (Cat. No. ALX-210-767) or a monoclonal antibody (Genox, Baltimore, MD; Cat. No. MHN-020P), as earlier described (22;23). Microsomal cytochrome p450 isoform 2E1 (CYP2E1) and isoform CYP1A2 were detected with antibodies from Abcam (CYP2E1 Cat. No. AP19140) and Santa Cruz (CYP1A2 Cat. No. sc-30085), as earlier described (24). p21/ WAF1/Cip1) was detected with mouse monoclonal antibody Cat. No. sc-6246 and rabbit polyclonal antibody Cat.No. sc-397 from Santa Cruz. Horseradish peroxidase-conjugated goat anti-rabbit or goat anti-mouse IgG (Jackson) was utilized for detection of binding by primary antibodies. Blots were developed with by enhanced chemiluminescence detection using the ECL Plus kit (Amersham/GE Healthcare Cat. No RPN2132). Automated densitometry was used to quantify the relative levels of protein expression using a Kodak Image Station 440CF with Kodak 1D Image Analysis Software (Eastman Kodak Company).

C-jun N-terminal kinase (JNK) assay. Liver tissue aliquots (~100 mg) was homogenized by

sonication in 400 µl of lysis buffer containing 20 mM Tris (pH 7.4), 150 mM NaCl, 1 mM EDTA, 1 mM EGTA, 1% Triton, 2.5 mM sodium pyrophosphate, 1 mM β-glycerolphosphate, 1 mM Na_3VO_4, 1 µg/ml Leupeptin, and 1mM phenylmethylsulfonyl fluoride (PMSF). JNK activity was tested by mixing 200 µg of liver lysate protein with agarose beads coupled to GST-c-Jun(1-89) fusion protein overnight at 4°C, followed by washing twice in lysis buffer, and incubating with 200 µM ATP in 50 µl of 25mM Tris (pH 7.5), 5mM β-glycerolphosphate, 2mM DTT, 0.1mM Na_3VO_4, 10mM $MgCl_2$ for 30 min at 30°C. Phosphorylation of GST-c-Jun(1-89) was detected by western blot analysis using anti-phospho-c-Jun (Ser63) antibody (Cell Signaling).

Pentose phosphate pathway (PPP) and connected metabolic enzyme activity assays.

Transaldolase (TAL) enzyme activity was tested in the presence of 3.2 mM D-fructose 6-phosphate, 0.2 mM erythrose 4-phosphate, 0.1 mM NADH, 10 ug α-glycerophosphate dehydrogenase/triosephosphate isomerase at a 1:6 ratio at room temperature by continuous absorbance reading at 340 nm for 20 min (25). The enzyme assays were conducted in the activity range of 0.001-0.01 U/ml. Transketolase (TK) activity was measured in 50 mM Tris-HCl pH 7.5, 5 mM $MgCl_2$, 0.06 mM thiamine pyrophosphate, 0.1 mM NADH, 10 ug α-glycerophosphate dehydrogenase/triosephosphate isomerase at a 1:6 ratio, 5 mM ribose 5-phosphate, and 1.25 mM xylulose 5-phosphate (26). Glucose 6-phosphate dehydrogenase (G6PD) activity was measured in the presence of 120 mM Tris pH 8.4, 10 mM $MgCl_2$, 2 mM glucose 6-phosphate, 0.9 mM NADP, and 0.1 U/ml 6PGD (27). Glutathione peroxidase (GPX) activity was measured in the presence of 150 mM KH_2PO_4 pH-7.0, 1 mM GSH, 0.25 mM NADPH, 3 U glutathione reductase, and 1 mM H_2O_2 (28). Catalase was measured in the presence of 50 mM

KH_2PO_4/Na_2HPO_4 pH-7.0 and 10 mM H_2O_2 at room temperature by continuous absorbance reading at 240 nm for 3 min (29). Gamma-glutamyl transferase (GGT) activity was measured in the presence of 1 mM L-gamma-Glutamyl-p-nitroanilide HCl, 20 mM glycylglycine, and 60 mM Tris-HCl pH 8.0 . The solutions are pre-incubated at 37 °C before assay. Reaction was initiated by addition of enzyme and the rate of release of p-nitro aniline was recorded at 410 nm (30). GTT from bovine kidney (Sigma) was used as positive control.

Measurement of phosphorylated sugars and nucleotides. All samples were analyzed following methanol/water extraction by LC-MS/MS (31). Sugar phosphates and nucleotides were detected in the same sample. NADH and NADPH were separately analyzed following extraction with KOH (15;31). This method allowed parallel detection of NADH (m/z 665), NADP (m/z 743), and NADPH (m/z 744) by CapLC/Q-TOF detection(31). ATP levels were also determined using the luciferin-luciferase method (32).

Microarray of gene expression. RNA was extracted from the liver using the RNeasy kit from Qiagen (Valencia, CA). The quality and quantity of the purified RNA was assessed using an Agilent 2100 Bioanalyzer (Waldbronn, Germany). The mRNA fraction in total RNA was reversed transcribed using an oligo-dT primer coupled to a T7 RNA polymerase recognition sequence using the Message Amp kit (Ambion, Austin, TX)). After second strand synthesis in the presence of RNase H, and subsequent DNA purification, approximately 2 μg of double-stranded cDNA was used as a template for in vitro transcription (IVT). During IVT, a fixed concentration of biotinylated CTP and UTP were incorporated into the cRNA products. After 4-6 hours, the IVT

reaction was stopped, and DNase 1 added to the tube to eliminate the template. 20 μg of biotinylated cRNA were hydrolyzed randomly to 35-200 nucleotides in a fragmentation buffer solution (94ºC, 35 min). 15 μg of the fragmented cRNA was then added to a hybridization buffer (100 mM 2-morpholinoethanesulfonic acid, 1 M [Na]+, 20mM EDTA, 0.01% Tween-20, 0.1mg/ml herring sperm DNA, 0.5 mg/ml acetylated BSA), containing known concentrations of positive control genes (50 pM Oligo B2, 1.5, 5, 25, and 100 pM of E. coli bioB, bioC, bioD, and cre). The entire hybridization solution was heated (99ºC, 5 min), equilibrated (45ºC, 5 min), and centrifuged at 15,000 g for 5 min, before being injected into a Mouse Expression Set 430A GeneChip containing 22,690 gene probe sets (Affymetrix). The GeneChips were hybridized at 45ºC for 16 hrs with constant rotation (60 rpm), then washed and stained on the Fluidics Station (Affymetrix) according to the EukGE-WS2 protocol. After washing and staining, fluorescent images were scanned at 2 micron resolution using the Agilent G2500A Gene Array Scanner.

Microarray Analysis Suite version 5.0 (Affymetrix) was used to determine the presence (P) or absence of a transcript (A), the differential change in gene expression [increase (I), decrease (D), marginal increase (MI), marginal decrease (MD), and no change (NC)], and the magnitude of change, which is represented as fold change. The mathematical definitions for each of these algorithms can be found in the Microarray Suite Analysis manual in the algorithm tutorial. Fold-change calculation was based on the average difference of each probe set owing to the fact that this output is directly related to its expression level. The fold change of any transcript between baseline and experimental value is calculated following global scaling, as described earlier (33).

After scanning the GeneChips, the Affymetrix software (MicroArray Suite 5.0) calculated the intensity of the signal from each perfect match probe relative to the signal for the mismatch

probe, and determined whether or not the gene was present in the sample (and a probability value associated with this determination: $p < 0.05$) as well as a measure of the expression level of the gene. Specifically, each chip was normalized to the distribution of all genes on the chip to control for variation between samples. The overall chip intensities for each sample were scaled by linear adjustment to the same target value (1,000). Each RNA from TAL+/- and TAL-/- mice was normalized to its specific control TAL+/+ littermates). Data were further transformed into log ratio for analysis and symmetry of distribution. Pivot tables containing the scaled data from each experiment were generated and imported into GeneSpring (Silicon Genetics). In GeneSpring, the individual gene chip data were normalized by adjusting the median intensity of each array to a value of 1.0. Gene expression patterns were then analyzed by determining the fraction of genes that were present in a sample and changed at specific fold change thresholds. Comparisons between genotypes were performed using one-way analysis of variance. Functional pathway analysis was performed by cross-annotating the mouse 430A gene chip content with the standard Simplified Gene Ontology (www.godatabase.org/chi-bin/go.cgi) and Kyoto Encyclopedia of Genes and Genomes databases (http://www.genome.ad.jp/kegg/), NetAffy (www.affymetrix.com), and the scientific literature. Differentially expressed genes were classified into functional categories based on the gene ontology definition.

Validation of gene expression by quantitative real time RT-PCR. Changes in selected RNA levels identified in the microarray analysis were validated by real-time PCR using the ABI PRISM® 7000 Sequence Detection System (Applied Biosystems). cDNAs were generated by reverse transcription and PCR analysis was performed using validated primer sets. The total RNA

was reverse transcribed using the ABI High Capacity cDNA archive kit (Applied Biosystems). Standard curves were made using serial dilutions from pooled cDNA samples. Real time PCR was performed using the SYBR Green PCR Master Mix (Applied Biosystems) according to the manufacturer's protocol and amplified on the ABI Prism 7000 sequence detection system. Three independent replicate RNA samples will be generated for each cell preparation. For the reverse transcription reaction, 500 ng of total RNA (in a 25 µl volume) from each RNA preparation is incubated with 250 picomoles of oligo $(dT)_{24}$ primer at 70ºC for 10 min. Then, 3.5 µl of 10 x PCR Gold buffer (Applied Biosystems), 15 µl of 25mM $MgCl_2$, 2 µl of 25mM dNTP, 0.5 µl of RNase inhibitor (40U/µl, Ambion), and 0.63 µl of SuperScript II RT (200U/µl, Invitrogen) are added. The reaction is incubated at 25ºC for 10 min, 48ºC for 30 min, terminated by heating to 95ºC for 5 min. For quantification of transcript differences, triplicate PCR reactions are performed for each gene of interest on 96 well plates. Each 25 µl PCR reaction contains 1 µl of diluted RT reaction, 1x TaqMan Universal PCR Master Mix and either validated Assay-on-Demand (Applied Biosystems) primer sets or 0.2 µM of each custom-designed forward and reverse primer, and 0.25 µl of SYBRGreenI dye (Molecular Probes). These reactions are cycled according to standard conditions. End point melt-curve analysis is used to confirm the presence of single amplicons in each reaction well and amplification in the absence of template is verified not to produce any signal due to primer dimerization and extension.The cycle threshold (CT) values corresponding to the PCR cycle number at which fluorescence emission in real time reaches a threshold above the base-line emission were determined. The Ct value assigned to a particular well thus reflects the point in the exponential phase of PCR reaction at which a sufficient number of amplicons have accumulated, in that well, to be at a statistically significant point above baseline. The CT was

directly proportional to the log of the copy number of the input DNA target sequence. Statistical analysis of the real time data is performed using a pairwise repeated measures ANOVA comparing the difference in the number of cycles to threshold (ΔC_T) between the transcript of interest and the reference gene β actin. Differences in expression levels between genotypes were calculated by determining the mean difference in the ΔC_T values per subject group ($\Delta\Delta C_T$), and a fold change calculated according to the formula: Fold Change = $2^{-\Delta\Delta CT}$.

Statistics. Results of parametric data are expressed as the mean ± standard error. Differences between TAL-deficient (TAL+/-, and TAL-/-) and control (TAL+/+) mice were determined by Student's t-test. Non-parametric data were analyzed with chi-square or Fisher's exact test for observations < 5. Survival curves were analyzed with the log rank test. P values were calculated with the Graphpad Software and considered significant at < 0.05.

REFERENCES

1. Perl,A., Qian,Y., Chohan,K.R., Shirley,C.R., Amidon,W., Banerjee,S., Middleton,F.A., Conkrite,K.L., Barcza,M., Gonchoroff,N. *et al*. 2006. Transaldolase is essential for maintenance of the mitochondrial transmembrane potential and fertility of spermatozoa. *Proc. Natl. Acad. Sci. USA* 103:14813-14818.

2. Picard,F., Wanatabe,M., Schoonjans,K., Lydon,J., O'Malley,B.W., and Auwerx,J. 2002. Progesterone receptor knockout mice have an improved glucose homeostasis secondary to

beta-cell proliferation. *Proc. Natl. Acad. Sci. USA* 99:15644-15648.

3. Ishak,K.G., Goodman,Z.D., and Stocker,J.T. 1999. Tumors of the Liver and Intrahepatic Bile Ducts. Armed Forces Institute of Pathology, Washington, DC,356 pp.

4. Anthony,P.P. 1994. Tumors and tumor-like lesions of the liver and biliary tract. In Pathology of the Liver. R.N.M.MacSween, Anthony,P.P., Scheuer,P.J., Burt,A.D., and Portmann,B.C., editors. Churchill Livingstone, London, Edinburgh, New York, pp 635-711.

5. Ferrell,L. 2000. Liver pathology: cirrhosis, hepatitis, and primary liver tumors. Update and diagnostic problems. *Mod. Pathol.* 13:679-704.

6. Zhao,L. and Burt,A. 2007. The diffuse stellate cell system. *J. Mol. Histol.* 38:53-64.

7. Berry,M.N. and Phillips,J.W. 2000. The isolated hepatocyte preparation: 30 years on. *Biochem. Soc. Trans.* 28:131-135.

8. Ni,R., Tomita,Y., Matsuda,K., Ichihara,A., Ishimura,K., Ogasawara,J., and Nagata,S. 1994. Fas-mediated apoptosis in primary cultured mouse hepatocytes. *Exp. Cell Res.* 215:332-337.

9. Banki,K., Hutter,E., Gonchoroff,N., and Perl,A. 1999. Elevation of mitochondrial transmembrane potential and reactive oxygen intermediate levels are early events and occur independently from activation of caspases in Fas signaling. *J. Immunol.* 162:1466-1479.

10. Tanner,M.K., Wellhausen,S.R., and Klein,J.B. 1993. Flow cytometric analysis of altered mononuclear cell transmembrane potential induced by cyclosporin. *Cytometry* 14:59-69.

11. Smiley,S.T., Reers,M., Mottola-Hartshorn,C., Lin,M., Chen,A., Smith,T.W., Steele,Jr.G.D., and Bo Chen,L. 1991. Intracellular heterogeneity in mitochondrial membrane potentials revealed by a J-aggregate-forming cation JC-1. *Proc. Natl. Acad. Sci. USA* 88:3671-3675.

12. Cossarizza,A., Franceschi,C., Monti,D., Salvioli,S., Bellesia,E., Rivabene,R., Biondo,L., Rainaldi,G., Tinari,A., and Malorni,W. 1995. Protective effect of N-acetylcysteine in tumor necrosis factor-α-induced apoptosis in U937 cells: The role of mitochondria. *Exp. Eye Res.* 220:232-240.

13. Mancini,M., Anderson,B.O., Caldwell,E., Sedghinasab,M., Paty,P.B., and Hockenbery,D.M. 1997. Mitochondrial Proliferation and Paradoxical Membrane Depolarization during Terminal Differentiation and Apoptosis in a Human Colon Carcinoma Cell Line. *J. Cell Biol.* 138:449-469.

14. Nagy,G., Koncz,A., and Perl,A. 2003. T cell activation-induced mitochondrial hyperpolarization is mediated by Ca^{2+}- and redox-dependent production of nitric oxide . *J. Immunol.* 171:5188-5197.

15. Banki,K., Hutter,E., Colombo,E., Gonchoroff,N.J., and Perl,A. 1996. Glutathione Levels and Sensitivity to Apoptosis Are Regulated by changes in Transaldolase expression. *J. Biol. Chem.* 271:32994-33001.

16. Kobzik,L., Godleski,J.J., and Brain,J.D. 1990. Oxidative metabolism in the alveolar macrophage: analysis by flow cytometry. *J. Leuk. Biol.* 47:295-303.

17. Rothe,G. and Valet,G. 1990. Flow cytometric analysis of respiratory burst activity in phagocytes with hydroethidine and 2',7'-dichlorofluorescin. *J. Leuk. Biol.* 47:440-448.

18. Carter,W.O., Narayanan,P.K., and Robinson,J.P. 1994. Intracellular hydrogen peroxide and superoxide anion detection in endothelial cells. *J. Leuk. Biol.* 55:253-258.

19. Hajnoczky,G., Robb-Gaspers,L.D., Seitz,M.B., and Thomas,A.P. 1995. Decoding of cytosolic calcium oscillations in the mitochondria. *Cell.* 82:415-424.

20. Banki,K., Halladay,D., and Perl,A. 1994. Cloning and expression of the human gene for transaldolase: a novel highly repetitive element constitutes an integral part of the coding sequence. *J. Biol. Chem.* 269:2847-2851.

21. Bohren,K.M., Grimshaw,C.E., and Gabbay,K.H. 1992. Catalytic effectiveness of human aldose reductase. Critical role of C- terminal domain. *J. Biol. Chem.* 267:20965-20970.

22. Terneus,M.V., Brown,J.M., Carpenter,A.B., and Valentovic,M.A. 2008. Comparison of S-adenosyl-l-methionine (SAMe) and N-acetylcysteine (NAC) protective effects on hepatic damage when administered after acetaminophen overdose. *Toxicology* 244:25-34.

23. Li,C.J., Nanji,A.A., Siakotos,A.N., and Lin,R.C. 1997. Acetaldehyde-modified and 4-hydroxynonenal-modified proteins in the livers of rats with alcoholic liver disease. *Hepatology* 26:650-657.

24. Pellinen,P., Stenback,F., Kojo,A., Honkakoski,P., Gelboin,H.V., and Pasanen,M. 1996. Regenerative changes in hepatic morphology and enhanced expression of CYP2B10 and

CYP3A during daily administration of cocaine. *Hepatology* 23:515-523.

25. Pontremoli,S., Prandini,D.B., Bonsignore,A., and Horecker,B.L. 1961. The preparation of crystalline transaldolase from Candida utilis. *Proc. Natl. Acad. Sci. USA* 47:1942-1955.

26. Heinrich,P.C., Morris,H.P., and Weber,G. 1976. Behavior of transaldolase (EC 2.2.1.2.) and transketolase (EC 2.2.1.1.) in normal neoplastic, differentiating, and regenerating liver. *Cancer Res.* 36:3189-3197.

27. Rudack,D., Chisholm,E.M., and Holten,D. 1971. Rat Liver Glucose 6-phosphate dehydrogenase. *J. Biol. Chem.* 246:1249-1254.

28. Wendel,A. 1981. Glutathione peroxidase. *Meth. Enzymol.* 77:325-333.

29. Lachaise,F., Martin,G., Drougard,C., Perl,A., Vuillaume,M., Wegnez,M., Sarasin,A., and Daya-Grosjean,L. 2001. Relationship between posttranslational modification of transaldolase and catalase deficiency in UV-sensitive repair-deficient Xeroderma pigmentosum fibroblasts and SV40-transformed human cells. *Free Radic. Biol. Med.* 30:1365-1373.

30. Meister,A., Tate,S.S., and Griffith,O.W. 1981. Gamma-glutamyl transpeptidase. *Meth. Enzymol.77:237-53*.

31. Vas,Gy., Conkrite,K., Amidon,W., Qian,Y., Banki,K., and Perl,A. 2005. Study of transaldolase deficiency in urine samples by capillary LC-MS/MS. *J. Mass. Spec.* 41:463-469.

32. Gergely,P.J., Niland,B., Gonchoroff,N., Pullmann,R.Jr., Phillips,P.E., and Perl,A. 2002. Persistent mitochondrial hyperpolarization, increased reactive oxygen intermediate production, and cytoplasmic alkalinization characterize altered IL-10 signaling in patients with systemic lupus erythematosus. *J. Immunol.* 169:1092-1101.

33. Middleton,F.A., Mirnics,K., Pierri,J.N., Lewis,D.A., and Levitt,P. 2002. Gene expression profiling reveals alterations of specific metabolic pathways in schizophrenia. *J. Neurosci.*. 22:2718-2729.

Table S1. PPP and antioxidant enzyme activities (mean ± SE mU/mg protein) in livers of seven female litters at 5-6 weeks of age. *, p value < 0.05, as compared to TAL+/+.

Enzyme	TAL+/+	TAL+/-	TAL-/-
Transaldolase	7.54+1.53	4.36±1.7*	0.3±0.53*
Transketolase	3.84±0.95	4.08±0.24	4.8±0.47
G6PD	1.13±0.12	1.27±0.15	0.68±0.09*
SOD	108.0±12.7	123.1±18.3	139.8±6.59*
CAT	3,293±403	6,402±381*	6,418±644*
GPx	2,854±343	4,222±192*	4,417±171*

Table S2. Microarray analysis of gene expression in microscopically normal liver of 5 week-old female mice from 4 litters using Mouse Expression Set 430A GeneChip containing 22,690 gene probe sets (Affymetrix, Santa Clara, CA). After scanning the GeneChips, the Affymetrix software (MicroArray Suite 5.0) was used to calculate the intensity of the signal from each perfect match probe relative to the signal for the mismatch probe and each chip was normalized to the distribution of all genes on the chip to control for variation between samples. The overall chip intensities for each sample were scaled by linear adjustment to the same target value (1.0).Each RNA from TAL+/- and TAL-/- mice was normalized to its specific control TAL+/+ littermate. Data were imported into GeneSpring, comparisons between genotypes were performed using one-way analysis of variance. Significant fold changes adjusted for multiple comparisons are shown, with respect to TAL+/+ control littermates. NC, no change.

Gene	Affymetrix	TAL	TAL-
TAL	1425129_a_	-1.7	-4.6
Gadd45g	1453851_a_	-4.9	-8.1
protein tyrosine phosphatase, non-receptor type 16/MAP kinase	1448830_at	+2.4	+3.3
tetratricopeptide repeat domain	1448361_at	+2.1	+8.5
glutathione-S-transferase, mu 2	1416411_at	+2.0	+2.1
growth arrest specific 2	1450112_a_	+2.0	+2.0
c-jun	1417409_at	+5.7	+8.0
N-myc downstream regulated 3	1417663_a_	+3.7	+5.7
C-type lectin	1424673_at	+9.2	+8.6
C-type lectin ligand	1431240_at	+4.3	+9.8
peroxisome proliferative activated receptor, gamma, coactivator 1	1437751_at	+1.3	+2.0
amino levulinate synthase	1451675_a_	+2.5	+4.9
Beclin-1	1439405_x_	+2.1	+4.3
ADP/ATP translocase 1/Adenine nucleotide translocator 1 (ANT 1)	1434897_a_	+1.6	+2.2

Table S3. Microarray analysis of gene expression in hepatomas of six TAL-/- mice in comparison to microscopically normal livers of four TAL-/- mice of 5 weeks of age. After adjusting for multiple comparisons, 18 genes were significantly downregulated $2-fold and 30 genes were significantly upregulated $2-fold in hepatomas with respect to normal TAL -/- livers.

Gene	Affymetrix ID	Fold change
major urinary protein 1	1426154_s_at	-6.49
cytochrome P450, family 2, subfamily f, polypeptide 2	1448792_a_at	-3.83
cytochrome P450, family 2, subfamily b, polypeptide 13	1449479_at	-3.81
transferrin receptor	X57349_M_at	-3.47
phosphoenolpyruvate carboxykinase 1, cytosolic	1423439_at	-3.35
cytochrome P450, family 2, subfamily b, polypeptide 9	1419590_at	-3.32
hepcidin antimicrobial peptide	1419196_at	-3.19
cytochrome P450, family 8, subfamily b, polypeptide 1	1449309_at	-2.93
hepcidin antimicrobial peptide	1419197_x_at	-2.89
glucose-6-phosphatase, catalytic	1417880_at	-2.84
cytochrome P450, family 2, subfamily b, polypeptide 20	1425645_s_at	-2.72
G0/G1 switch gene 2	1448700_at	-2.36
cytochrome P450, family 2, subfamily e, polypeptide 1	1415994_at	-2.27
thioredoxin interacting protein	1415996_at	-2.14
aldehyde dehydrogenase 2, mitochondrial	1434987_at	-2.07
cytochrome P450, family 3, subfamily a, polypeptide 44	1426064_at	-2.01
RAS protein-specific guanine nucleotide-releasing factor 1	1435614_s_at	-2.00
regucalcin	1448852_at	-2.00
AP1 gamma subunit binding protein 1	AFFX-MURINE_B2_at	+5.7
lectin, galactose binding, soluble 1	1455439_a_at	+3.6
CREBBP/EP300 inhibitory protein 1	1448405_a_at	+3.8
SRY-box containing gene 4	1433575_at	+3.2
pyruvate carboxylase	L09192_MB_at	+2.4
lectin, galactose binding, soluble 3	1426808_at	+3.8
aldolase 1, A isoform	1434799_x_at	+2.1
RAB6, member RAS oncogene family	1447776_x_at	+2.3
Ras association (RalGDS/AF-6) domain family 4	1444009_at	+2.2
xanthine dehydrogenase	1424609_a_at	+2.1
NAD(P)H dehydrogenase	1423627_at	+2.2
Ewing sarcoma breakpoint region 1	1436884_x_at	+2.1
phosphogluconate dehydrogenase	1436771_x_at	+3.2
lectin, galactose binding, soluble 1	1419573_a_at	+2.7
procollagen, type IV, alpha 1	1452035_at	+2.6
transglutaminase 2, C polypeptide	1433428_x_at	+2.8
B-cell leukemia/lymphoma 2 related protein A1d	1419004_s_at	+3.2
Jun-B oncogene	1415899_at	+2.1
zinc finger proliferation 1	1449732_at	+2.3
glutathione S-transferase, mu 3	1427474_s_at	+2.7
v-ral simian leukemia viral oncogene homolog B (ras related)	1435517_x_at	+2.3
aldo-keto reductase family 1, member B3 (aldose reductase)	1437133_x_at	+2.5
glutathione peroxidase 3	1449106_at	+2.7
tetratricopeptide repeat domain 13	1438631_x_at	+2.1
PRKC, apoptosis, WT1, regulator	1426910_at	+2.1
caspase 12	1449297_at	+2.3
transforming growth factor, beta receptor II	1426397_at	+2.2
fos-like antigen 2	1437247_at	+2.5
alpha fetoprotein	1416645_a_at	+2.6
caspase 1	1449265_at	+2.1

LEGENDS TO SUPPLEMENTARY FIGURES

Figure S1. Glucose tolerance testing of seven TAL+/+, TAL+/-, and TAL-/- female littermates of 10-12 weeks of age. After overnight (~14h) fasting, mice were injected ip with 2 g/kg sterile-filtered glucose. A single drop of blood was obtained through needle-pricking of the tail vein and glucose levels were assessed before and 15, 30, 60, and 120 min after injection. The overall difference in glucose levels between TAL+/+ and TAL-/- mice for all time points was significant at $p = 0.048$. The 30 min time point showed the greatest statistically significant difference between TAL+/+ and TAL -/- mice with *t*-test ($p < 0.0001$).

Figure S2. Transmission electron microscopy of the liver from 12 week-old TAL+/+ and TAL-/- littermate mice. Original magnifications were 2,900-fold for panel A, 11,000-fold for panel B, 13,000-fold for panel C, and 18,000-fold for panel D. The nucleus (N), mitochondria (M) and lipid droplets (L) are labeled in images of higher magnification. TAL-/- hepatocytes showed accumulation of lipid droplets and diminished size and numbers of mitochondria.

Figure S3. Assessment of cell proliferation by detecting expression of proliferating cell nuclear antigen (PCNA). A, PCNA-positive nuclei per 1,000 hepatocytes were assessed in the liver of three sets of 8-week-old TAL+/+, TAL+/-, and TAL-/- littermates and they are represented on the left Y axis. PCNA-positive nuclei per 1,000 hepatocytes in three TAL-/- hepatomas (HEP) are represented on the right Y axis. p values < 0.05 are indicated. B, Immunohistochemical detection of PCNA in livers of TAL+/+, TAL+/-, and TAL-/- littermates and in a TAL-/- HCC. 6 indicates

a representative PCNA-positive nucleus in TAL+/- and TAL-/- livers and TAL-/- HCC. Sections were photographed at a 100-fold original magnification.

Figure S4. Detection of lipid hydroperoxides (LPO) and malondialdehyde (MDA) and 4-hydroxynonenal (4-HNE) adducted proteins in liver tissues. A) LPO levels in liver of TAL+/+, TAL+/-, and TAL-/- littermates. Triplicates of liver tissues (~200 mg) were homogenized in 500 µl of HPLC-grade water and, after addition of 500 µl of extract-R-saturated methanol, extracted with 1 ml of deoxygenated chloroform. 700 µl of chloroform extract was assayed for LPO content relative to a standard calibration curve following the manufacturer's instructions. Data show mean ± SEM of three sets of 10-14-week-old TAL+/+, TAL+/-, TAL-/- littermates. LPO levels were increased in TAL+/- and TAL-/- livers relative to TAL+/+ controls (*, $p < 0.05$). B, Western blot detection of 4-HNE and MDA-adducted proteins in livers of 10-week-old female TAL+/+, TAL+/-, and TAL-/- littermates. 4-HNE (left panel) and MDA protein adducts (middle panel) were detected and shown in the molecular size range of 30-110 kD and quantified relative to actin using automated densitomery. The blot probed with anti-MDA antibody was reprobed with TAL and actin antibodies (right panel). NAC-treated mice were supplemented with 10 g/l NAC in drinking water from conception. Values were normalized to that of TAL+/+ mice fed with regular water.

Figure S5. Assessment of microsomal CYP2E1 and CYP1A2 protein levels relative to β-actin in the liver of two female and two male sets of TAL+/+, TAL+/-, and TAL-/- littermates by western blot analysis. CYP2E1/actin levels were similar in the liver of TAL+/+ (normalized at 1.0 ± 0.05),

TAL+/- (1.2 ± 0.3 %; p=0.33) and TAL-/- (1.0 ± 0.1 %; p=0.95) mice. CYP1A2/actin levels were similar in the liver of TAL+/+ (normalized at 1.0 ± 0.02), TAL+/- (1.1 ± 0.2 %; p=0.84) and TAL-/- (0.9 ± 0.3 %; p=0.79) littermates.

Figure S6. Effect of JNK inhibitor SP600125 on acetaminophen (acetyl-p-aminophenol or APAP) -induced liver failure in TAL-/- mice. Survival of six mice pre-treated with 30 mg/kg SP600125 was compared to the survival of six mice pre-treated with an equal volume/body weight of solvent alone (Control) 1 h prior to exposure to 800 mg/kg APAP (p=0.56).

Figure S7. Effect of life-long NAC treatment (10 g/l NAC in drinking water) on Fas-induced death. Survival of six NAC-treated TAL-/- mice was compared to seven untreated TAL-/- mice of 10-12 weeks of age, following intra-peritoneal injection with Fas-specific Jo2 hamster monoclonal antibody (10 μg/30 g body weight).

Figure S8. Steatosis in 52-week-old TAL+/- and TAL-/- mice relative to TAL+/+ littermate control after life-long NAC treatment. Hematoxylin and eosin-stained sections were photographed at a 100-fold original magnification.

Figure S9. Schematic diagram of the molecular basis of liver disease in TAL deficiency. A, Metabolic consequences of TAL deficiency. Under normal conditions, the oxidative phase of the PPP produces two NADPH molecules per G6P. TAL, an enzyme of the non-oxidative phase, catalyzes the transfer of dihydroxyacetone from S7P and F6P to GA3P and E4P, respectively.

Forward reaction of TAL recycles R5P into G6P (upward arrow); reverse TAL reaction promotes metabolism of G6P into R5P (downward arrow). TAL deficiency leads to accumulation of S7P, R5P, X5P, RU5P, C5-polyols (D-ribitol/D-arabitol/D-xylitol), ADP-ribose (red/upward arrows), and depletion of G6P and NADPH (blue/downward arrows). Thus, TAL deficiency blocks the forward reaction and recycling of R5P to G6P. R5P, X5P, and RU5P inhibit 6PGD, while elevation of the total adenine nucleotide pool (AMP, ADP and ATP) inhibit both G6PD and 6PGD. Excess R5P (X5P and RU5P) can be converted to ribose by ribose-5-phosphatase, which is then reduced to ribitol by AR, thus further depleting NADPH. GSH reductase uses NADPH to regenerate GSH from GSSG. NADPH and GSH depletion cause oxidative stress. Depletion of GSH inhibits Fas apoptosis by curtailment of caspase activity. Oxidative stress and C5-sugars and C5-polyols stimulate JNK activity and c-jun expression which in turn promote expression of AFP and hepatocyte proliferation. B, Schematic diagram of the hepatocarcinogenesis in TAL-deficient mice. Reduced NADPH and GSH levels causes Fas resistance, JNK/c-jun activation and hepatocarcinogenesis. NAC normalizes GSH and reverses Fas resistance, blocks JNK/c-jun activation, and prevents hepatocarcinogenesis.

Abbreviations: 3K6PG, 3-keto-6-phosphogluconate; 6PG, 6-phosphogluconate; 6PGD, 6-phosphogluconate dehydrogenase; AFP, alpha-fetoprotein; AR, aldose reductase; E4P, erythrose 4-phosphate; F6P, fructose 6-phosphate; FGI, phosphoglocose isomerase; G6P, glucose 6-phosphate; G6PD, glucose 6-phosphate dehydrogenase; GA3P, glyceraldehyde 3-phosphate; GLH, gluconolactone hydrolase; Ri5P, ribitol 5-phosphate; Ri5Pase, ribitol 5-phosphatase; R5P, ribose 5-phosphate; R5Pase, ribose 5-phosphatase; R5PKI, ribulose 5-phosphate ketoisomerase; RU5P, ribulose 5-phosphate; RU5P3E, ribulose 5-phosphate-3-epimerase; S1,7P, sedoheptulose

1,7-biphosphate; S7P, sedoheptulose 7-phosphate; TAL, transaldolase; TK, transketolase; X5P, xylulose 5-phosphate.

Figure S1

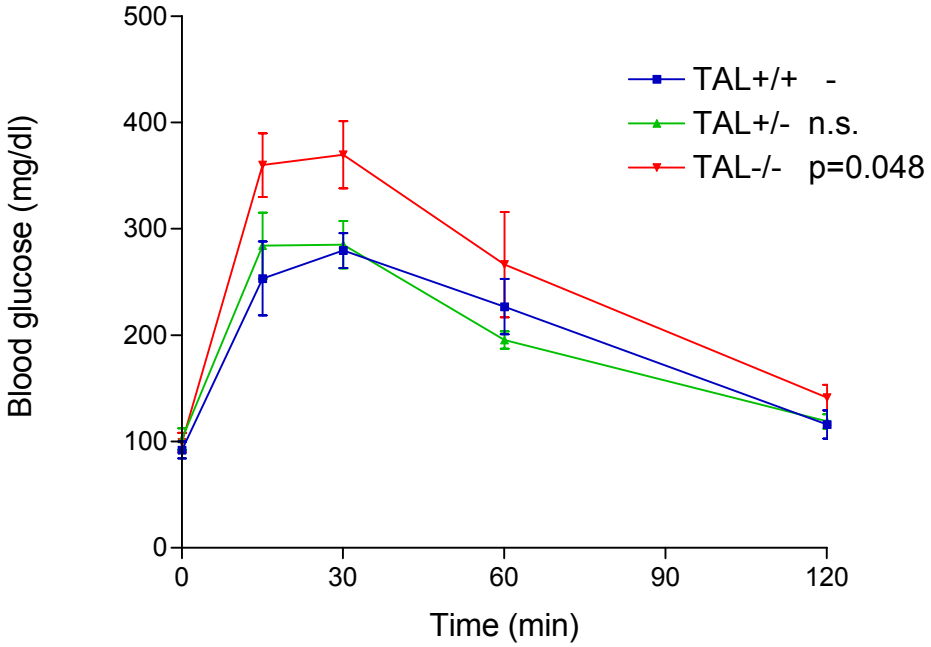
Blood glucose (mg/dl)
500
400
300
200
100
0
0
30
60
90
120
Time (min)
TAL+/+ -
TAL+/- n.s.
TAL-/- p=0.048

Figure S2

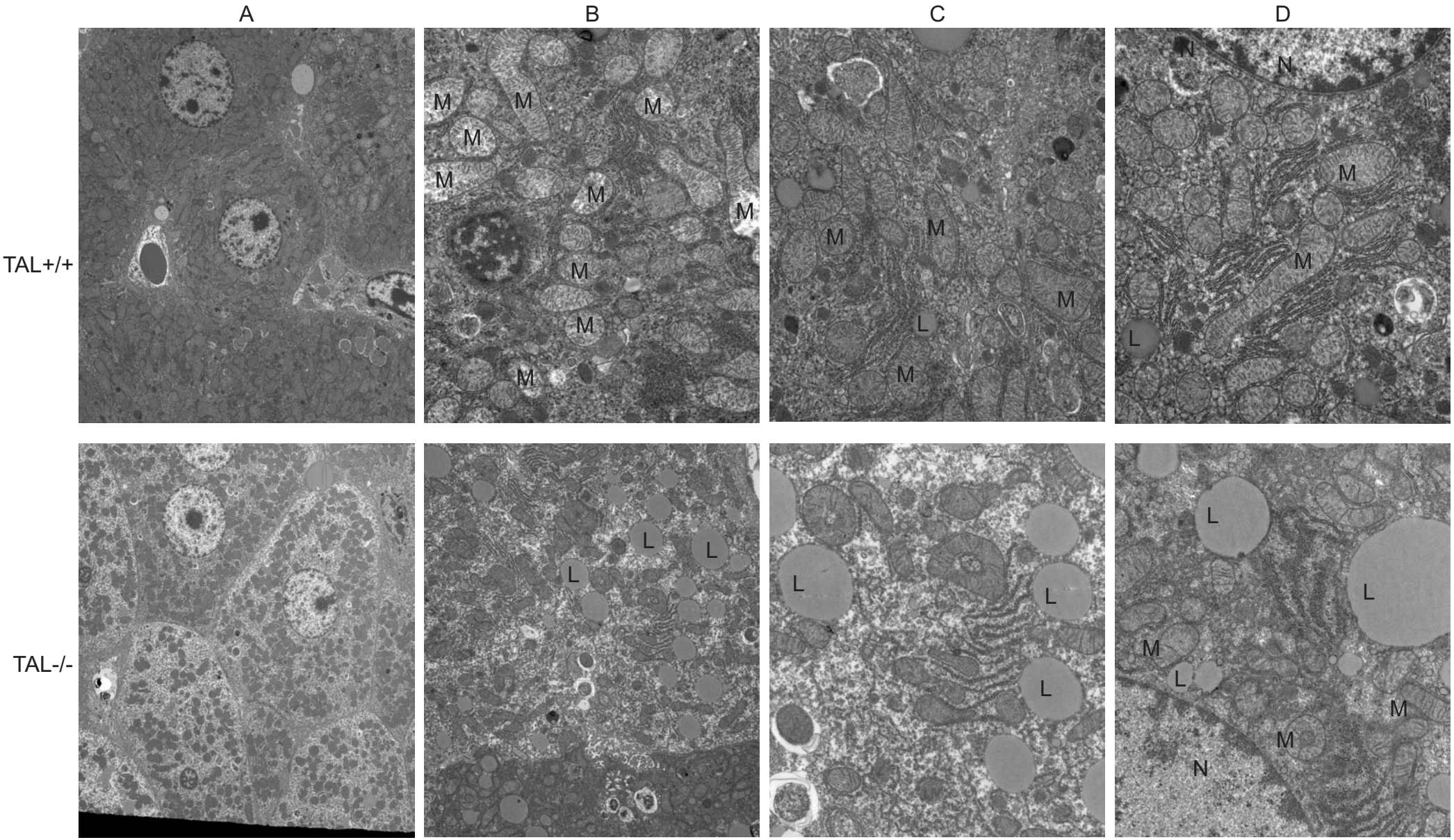

Figure S3

A

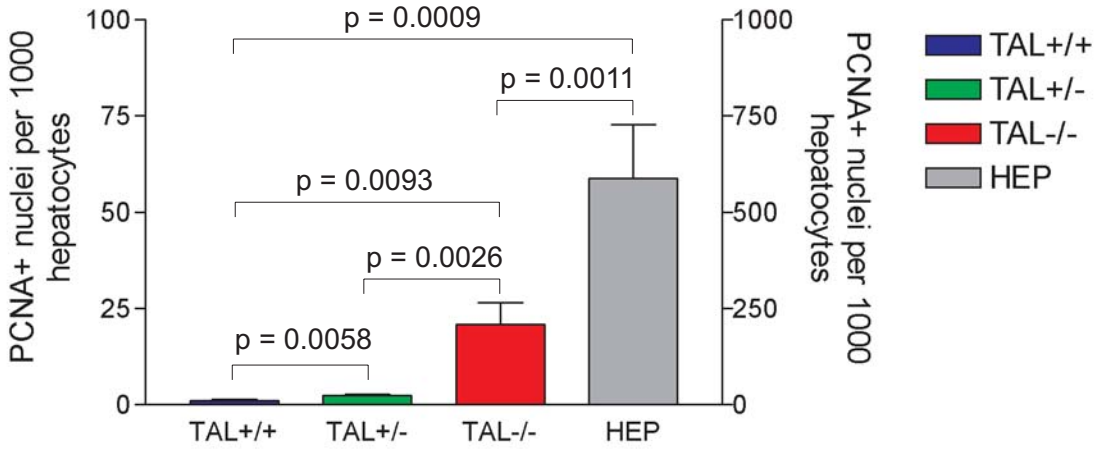
p = 0.0009
p = 0.0011
p = 0.0093
p = 0.0026
p = 0.0058
PCNA+ nuclei per 1000 hepatocytes
100
75
50
25
0
1000
750
500
250
0
TAL+/+
TAL+/-
TAL-/-
HEP
PCNA+ nuclei per 1000 hepatocytes
TAL+/+
TAL+/-
TAL-/-
HEP

B

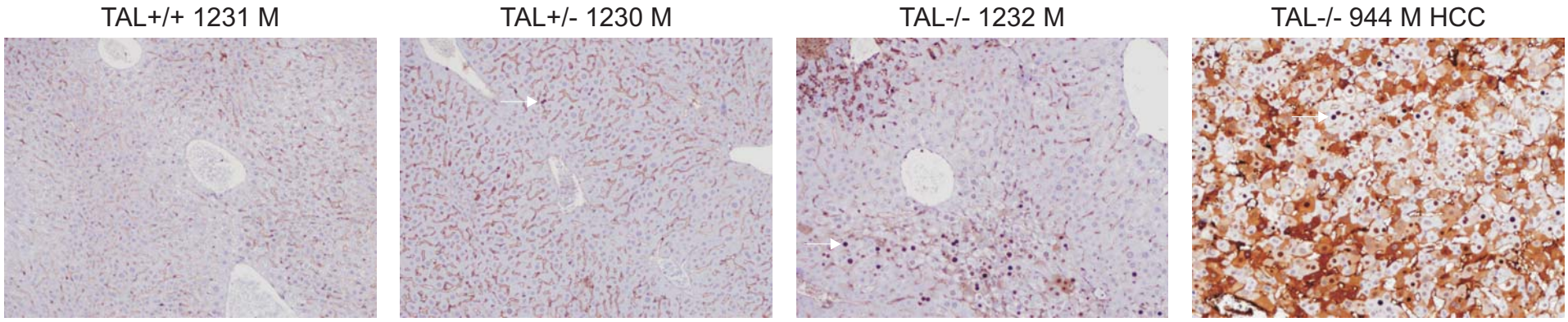
TAL+/+ 1231 M
TAL+/- 1230 M
TAL-/- 1232 M
TAL-/- 944 M HCC

Figure S4

A

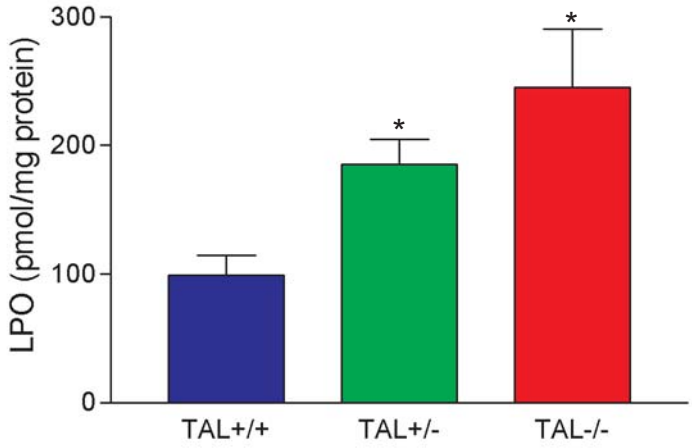
LPO (pmol/mg protein)
300
200
100
0
*
*
TAL+/+
TAL+/-
TAL-/-

B

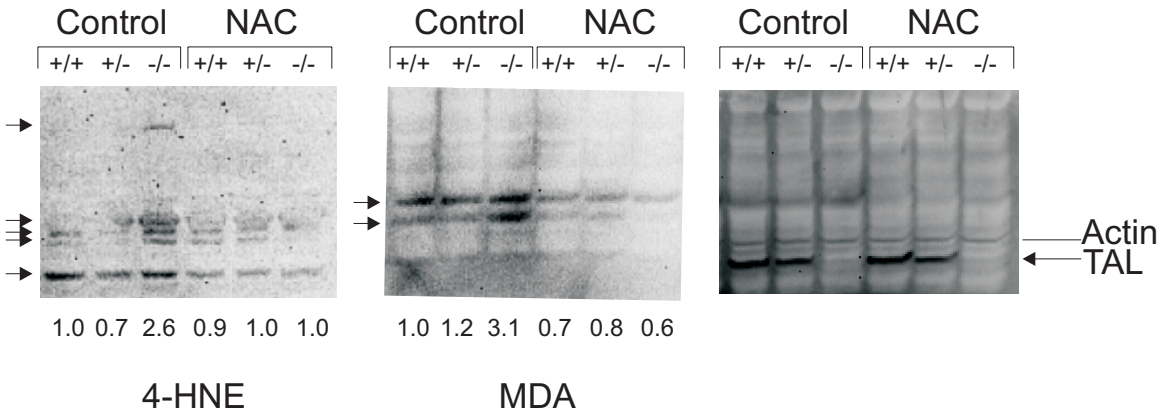
Control
NAC
Control
NAC
Control
NAC
+/+ +/- -/- +/+ +/- -/-
+/+ +/- -/- +/+ +/- -/-
+/+ +/- -/- +/+ +/- -/-
Actin
TAL
1.0 0.7 2.6 0.9 1.0 1.0
1.0 1.2 3.1 0.7 0.8 0.6
4-HNE
MDA

Figure S5

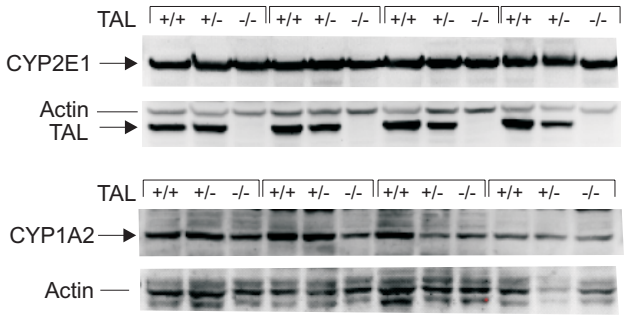

Figure S6

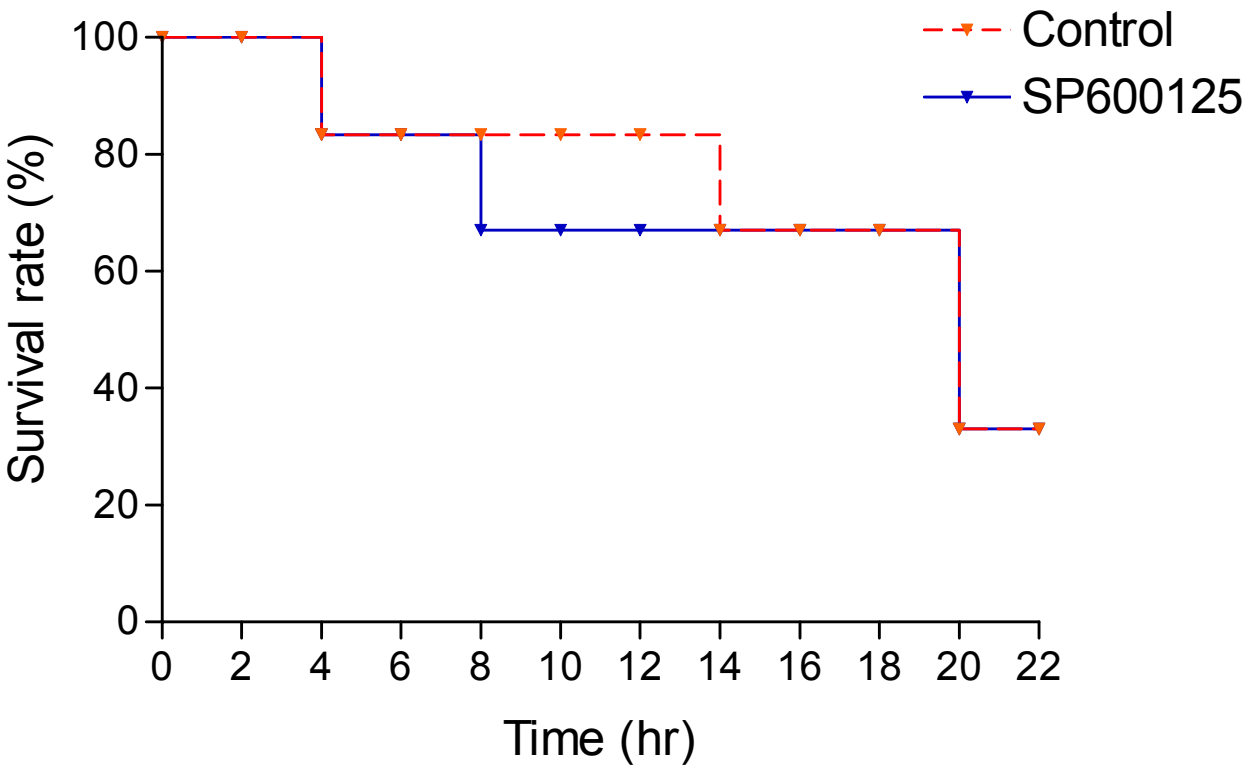
Control
SP600125
Survival rate (%)
100
80
60
40
20
0
0
2
4
6
8
10
12
14
16
18
20
22
Time (hr)

Figure S7

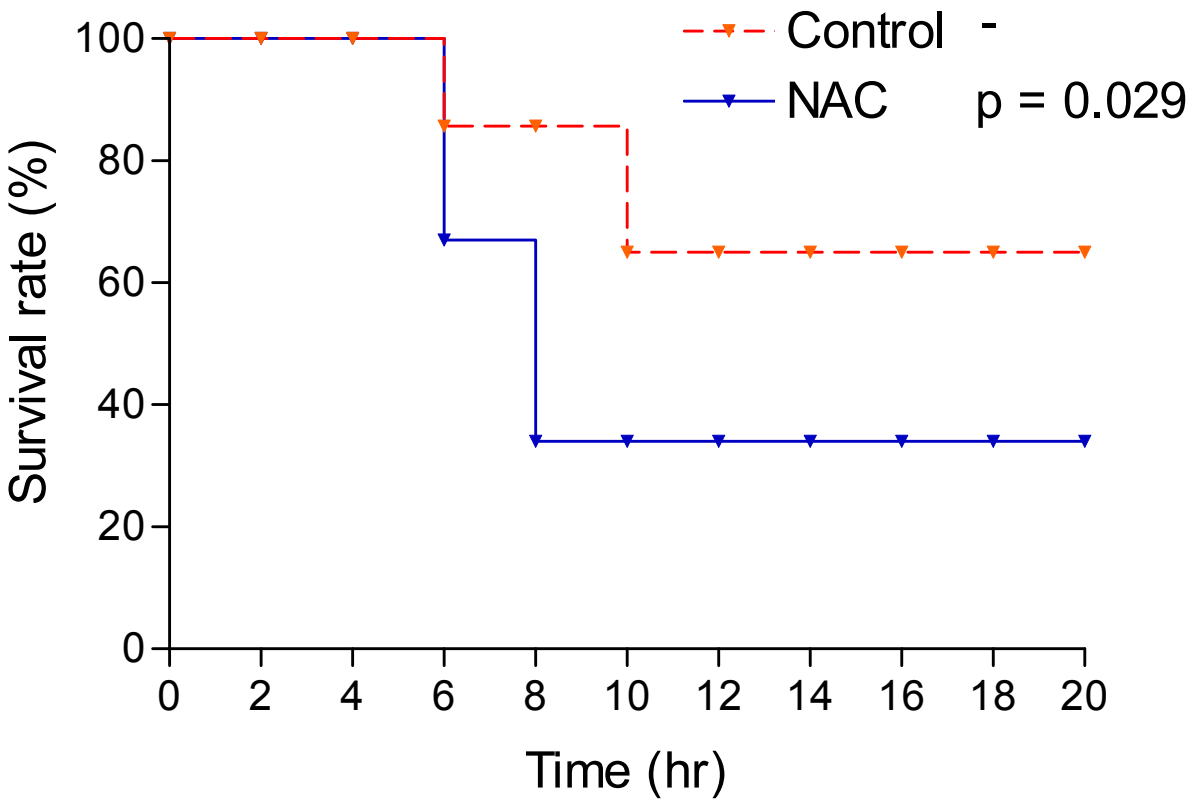
Control -
NAC p = 0.029
Survival rate (%)
100
80
60
40
20
0
0 2 4 6 8 10 12 14 16 18 20
Time (hr)

Figure S8

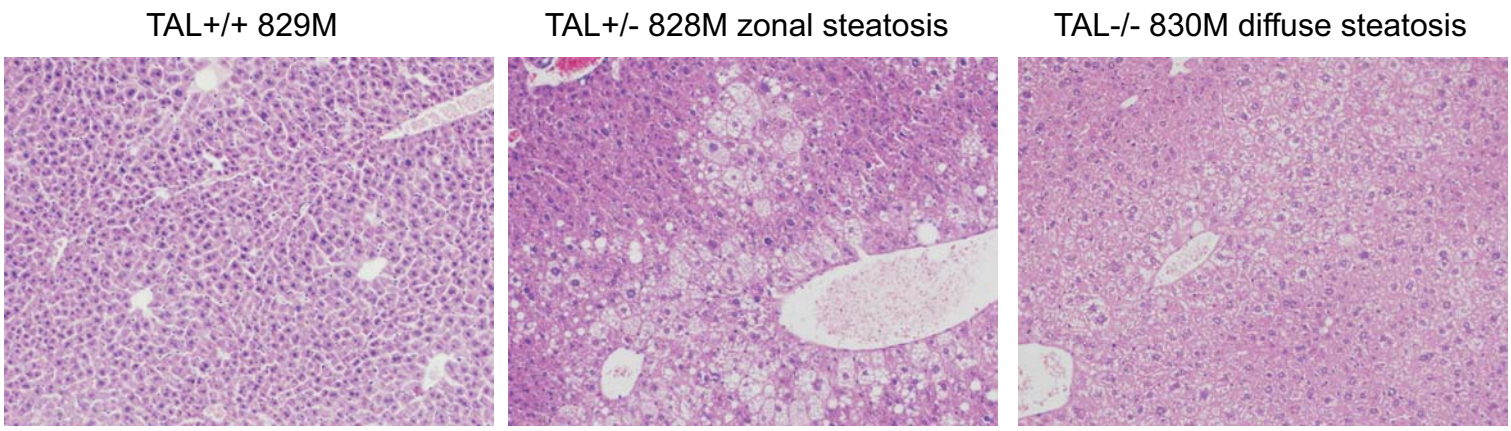
TAL+/+ 829M
TAL+/- 828M zonal steatosis
TAL-/- 830M diffuse steatosis

Figure S9

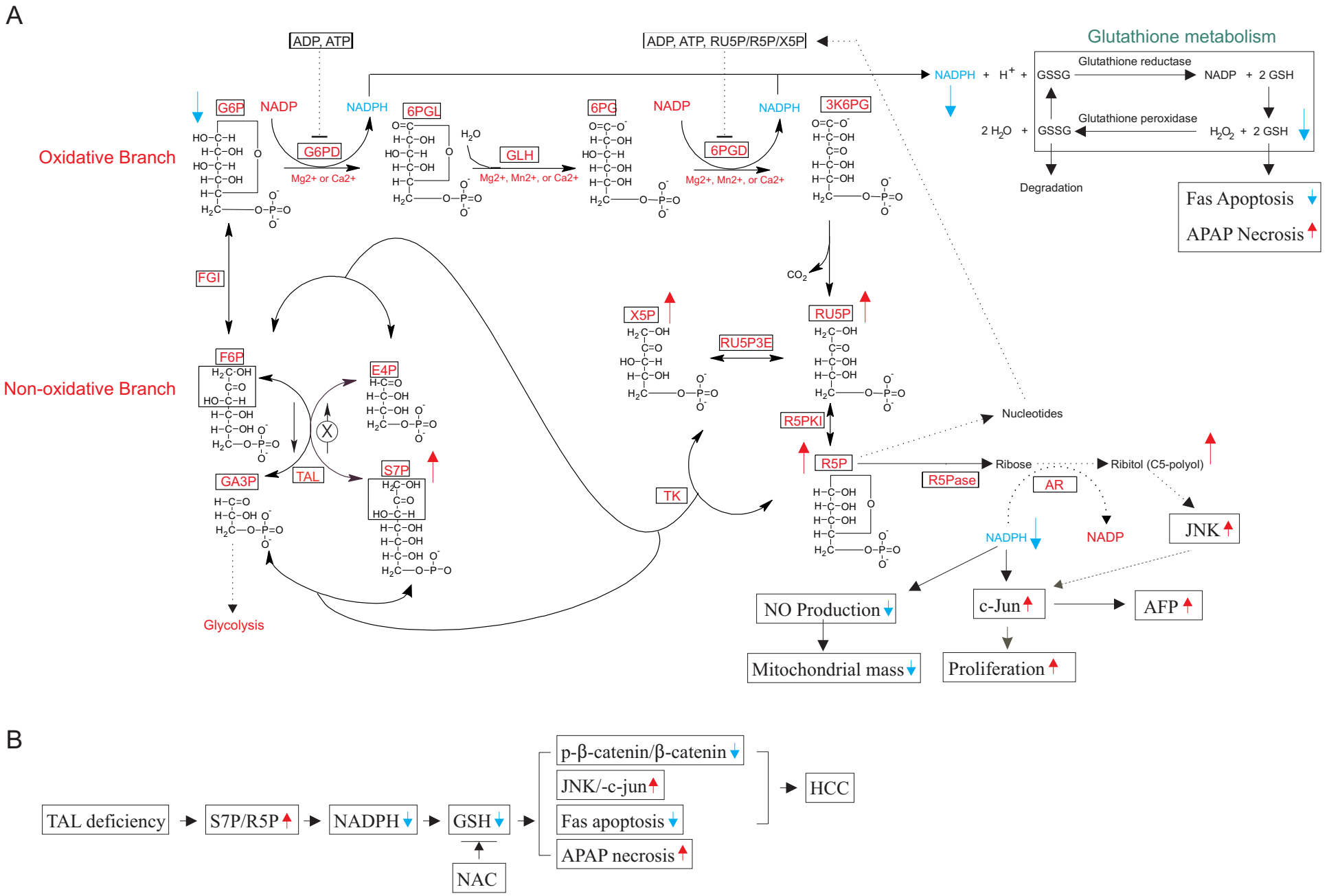
A
Oxidative Branch
Non-oxidative Branch
ADP, ATP
ADP, ATP, RU5P/R5P/X5P
G6P
NADP
NADPH
G6PD
Mg2+ or Ca2+
6PGL
GLH
Mg2+, Mn2+, or Ca2+
6PG
6PGD
3K6PG
FGI
F6P
E4P
GA3P
TAL
S7P
X5P
RU5P3E
RU5P
R5PKI
R5P
R5Pase
Ribose
Ribitol (C5-polyol)
AR
Nucleotides
TK
Glycolysis
Glutathione metabolism
Glutathione reductase
Glutathione peroxidase
GSSG
NADP + 2 GSH
2 H2O + GSSG
H2O2 + 2 GSH
Degradation
Fas Apoptosis
APAP Necrosis
JNK
NO Production
Mitochondrial mass
c-Jun
AFP
Proliferation
B
TAL deficiency
S7P/R5P
NADPH
GSH
NAC
p-β-catenin/β-catenin
JNK/-c-jun
Fas apoptosis
APAP necrosis
HCC